

# 1 **Realism of Local and Remote Feedbacks on Tropical Sea Surface** 2 **Temperatures in Climate Models**

3

4 **Sang-ik Shin\***, Prashant D. Sardeshmukh, and Kathy Pegion5 *CIRES Climate Diagnostics Center, University of Colorado and NOAA Earth System Research*  
6 *Laboratory, Boulder, Colorado, USA*

7

8 ***Journal of Geophysical Research - Atmosphere*** (submitted: Jan. 2010)

9

10 **Abstract**

11 An important emerging issue in climate research is the degree to which a Sea Surface  
12 Temperature (SST) change in one tropical ocean basin affects the SST in other basins. In this  
13 study the SST interactions among 8 broadly defined regions of coherent SST variability in the  
14 tropical Pacific, Indian, and Atlantic oceans are estimated using 3 observational and 76 climate  
15 model simulation datasets of the 20<sup>th</sup> century. The 8-dimensional SST feedback matrix is  
16 estimated separately using each dataset by constructing a Linear Inverse Model based on the lag-  
17 covariance statistics of the 100-yr monthly SST time series. The simulated feedback matrices are  
18 found to differ in several key respects from the observed matrices, and also from one another. In  
19 particular, the influence of the eastern Pacific ENSO region on other regions, and of the other  
20 regions on the ENSO region, are found to vary considerably from model to model. The  
21 representation of remote interactions with the Indo-Pacific Warm Pool region is also found to be  
22 highly variable. It is argued that these large errors/differences arise mainly from differences in

---

\* Current affiliation: College of Marine Science, University of South Florida, 140 7th Ave. S., St. Petersburg, FL.

23 the representation of the remote atmospheric teleconnective feedbacks, and to a lesser extent the  
24 local radiative-thermodynamic feedbacks, on the SSTs in the models, whereas differences in the  
25 representation of the tropical oceanic wave dynamics are likely less important.

26

27

## 28 **1. Background**

29 Most climate models remain deficient at representing important atmospheric and oceanic aspects  
30 of the tropical climate. For example, the simulated atmospheric intertropical convergence zone  
31 (ITCZ) varies considerably from model to model, with many models generating an unrealistic  
32 “double ITCZ” structure, and in many oceanic simulations a 1-2 K mean SST bias is found over  
33 large areas [e.g. Lin 2007]. The ultimate origin of such biases remains a mystery. At least in part,  
34 this is because it is still unclear how a change and/or error in one part of the system causes a  
35 change and/or error in another part, and what overall effect this has on the simulation and  
36 prediction of tropical climate variations.

37

38 In this study, we attempt to address the first part of this question. We are especially interested in  
39 how the SST variations in the Indian, Pacific, and Atlantic Ocean basins are interlinked.  
40 Although these basins are separated from each other by the American and African land masses  
41 and the Maritime Continent, their interactions with each other, which occur predominantly  
42 through the atmosphere on time scales of a few months, can nevertheless be substantial. For  
43 example, it is well recognized that El Niño related SST variations in the eastern equatorial  
44 Pacific influence climate variability over the adjacent oceans [e.g. Enfield and Mayer 1997;  
45 Penland and Matrosova 1998; Klein et al. 1999; Alexander et al. 2002; Giannini et al. 2004].

46 Conversely, the relatively weak SST variability in the Indian and Atlantic basins also modifies  
47 ENSO variability in the Pacific basin [Yu et al. 2002; Annamalai et al. 2005; Kug and Kang  
48 2006; Kug et al. 2006; Dommenges et al. 2006; Yeh et al. 2007]. The question naturally arises,  
49 how accurately do current coupled climate models capture such interactions among these ocean  
50 basins?

51  
52 We are also interested here in the dominant interactions *within* each of these basins, especially  
53 between the eastern and western and off-equatorial and equatorial Pacific, between the northern  
54 and southern tropical Atlantic, and between the western and eastern Indian oceans. We suspect --  
55 and confirm below -- that these interactions are also not well represented in climate models,  
56 partly because (with the possible exception of east-west interactions in the equatorial Pacific)  
57 they are not dominated by well-understood oceanic wave dynamics. Even within the equatorial  
58 Pacific zone, there are questions concerning how well climate models capture the east-west SST  
59 interactions associated with fluctuations of the atmospheric Walker circulation, which are an  
60 integral part of the ENSO phenomenon.

61  
62 Guided by EOF analyses of observed monthly SST variations in each basin, we selected a total  
63 of 8 geographically localized regions in the tropics (30°S-30°N) among which to investigate the  
64 SST interactions (see Fig. 1). We focused on the *effectively linear feedbacks* among these  
65 regions, encapsulated in an 8×8 deterministic system feedback matrix  $\mathbf{L}$ , by constructing and  
66 intercomparing the  $\mathbf{L}$  matrices obtained from Linear Inverse Modeling [LIM; see e.g. Penland  
67 and Sardeshmukh 1995, Newman et al. 2009] of both observed and simulated monthly tropical  
68 SST variations over the 20<sup>th</sup> century (1900-1999). We constructed three observationally based  $\mathbf{L}$

69 matrices using SST datasets compiled at the Hadley Centre of the UK Met Office [HadISST;  
 70 Rayner et al. 2003], the Lamont-Doherty Earth Observatory [Kaplan et al. 1998], and the  
 71 National Oceanic and Atmospheric Administration [NOAA, Smith and Reynolds 2005]. We then  
 72 compared these matrices with 76  $\mathbf{L}$  matrices derived from 76 coupled model simulations of the  
 73 20th century, available at the Program for Climate Model Diagnosis and Intercomparison  
 74 (PCMDI; <http://www-pcmdi.llnl.org>). These simulations were generated using prescribed  
 75 observed time-varying radiative forcings associated with greenhouse gases, aerosols, and solar  
 76 variations as part of the Climate of the Twentieth Century project (20C3M), as a contribution to  
 77 the Fourth Assessment Report (AR4) of the Intergovernmental Panel on Climate Change [IPCC  
 78 2007].

79

## 80 **2. Diagnosis method**

81 Our multivariate diagnosis of tropical SST interactions rests on approximating the evolution of  
 82 tropical variations on longer than weekly time scales by a linear stochastically forced model of  
 83 the form,

$$84 \quad \frac{d\mathbf{x}}{dt} = \mathbf{L}\mathbf{x} + \mathbf{B}\eta + \mathbf{F}, \quad (1)$$

85 where  $\mathbf{x}(t)$  is the  $N$ -component system state vector with  $N=8$  components representing the  
 86 spatially averaged monthly-mean SST anomalies in our 8 regions, all predictable dynamical  
 87 interactions among the system components are represented in the  $N \times N$  deterministic linear  
 88 feedback matrix  $\mathbf{L}$  (sometimes also called the system sensitivity matrix or the matrix of time  
 89 scales), and all unpredictable chaotic nonlinear dynamics are approximated by the stochastic  
 90 forcing  $\mathbf{B}\eta$ , where  $\eta$  is an  $M$ -component noise vector of independent white noises and  $\mathbf{B}$  is a

91 constant  $N \times M$  matrix. Note that the expected mean  $\langle \mathbf{B}\eta \rangle$  of this stochastic forcing is zero. The  
 92  $N$ -component vector  $\mathbf{F}$  represents external radiative forcing of the system.

93

94 It is important to recognize that although (1) is formulated using only SST, it implicitly includes  
 95 influences of other climate variables such as winds and ocean currents on SST, and also  
 96 nonlinear effects, in approximate form. Specifically, deterministic interactions with other  
 97 variables are implicitly included in  $\mathbf{L}$  to the extent that those variables can be linearly diagnosed  
 98 from the monthly SST anomaly state vector. As for nonlinear effects, the basic premise in (1)  
 99 concerning the evolution of monthly SST anomalies is that the nonlinear SST tendency terms  
 100 associated with submonthly SST anomalies and fluxes are in principle linearly parameterizable  
 101 in terms of the monthly SSTs, and the unparameterized remainder can be treated as stochastic  
 102 white noise. With these approximations in mind, it is apparent that  $\mathbf{L}$  in (1) is not that obtained  
 103 by directly linearizing the governing fluid dynamical equations but also includes such linear  
 104 interactions with other variables and linear parameterizations of unresolved processes, and  $\mathbf{B}$   
 105 accounts for the amplitude and spatial correlation structure of the unparameterized remainder as  
 106 a “stochastic parameterization”. We interpret  $\mathbf{L}$  as an *effectively linear feedback matrix*  
 107 governing monthly SST variations in the tropics. Each of its elements  $L_{ij}$  quantifies the direct  
 108 dynamical influence (in a dynamical systems sense) of the SST  $x_j$  in region  $j$  on the SST  $x_i$  in  
 109 region  $i$ , as distinct from additional indirect influences of region  $j$  on region  $i$  via other regions  $k$ .  
 110 Note that in general  $L_{ij} \neq L_{ji}$ . Note also that because the system is multivariate, the  $L_{ij}$  are not  
 111 simply identical to the regression coefficients of  $x_i$  on  $x_j$ .

112

113 The approximation (1) may be justified using several lines of evidence. First, many coupled  
 114 climate models are found to respond approximately linearly to imposed GHG and other external  
 115 radiative forcing changes on decadal and longer timescales [e.g., Meehl et al. 2004; Cash et al.  
 116 2005; Knutson et al. 2006 and references therein], consistent with a linear ensemble-mean  
 117 response  $\langle \mathbf{x} \rangle = -\mathbf{L}^{-1}\mathbf{F}$  that one would predict using (1). Second, on shorter interannual scales on  
 118 which the changes of  $\mathbf{F}$  are relatively small, the SST dynamics are consistent with those of a  
 119 stochastically forced linear system both in the tropics [Penland and Sardeshmukh 1995, Newman  
 120 et al. 2009] and the extratropics [Hasselmann 1976; Frankignoul 1985; Barsugli and Battisti  
 121 1998, Alexander et al. 2008]. Several studies have also shown that the predictable global  
 122 atmospheric dynamics on these time scales are dominated by linear global responses to tropical  
 123 SST variations [e.g. Barsugli and Sardeshmukh 2002; Schneider et al. 2003; Barsugli et al.  
 124 2006]. Indeed, on these time scales it is difficult to improve upon predictions based on empirical  
 125 linear correlations, using even state-of-the-art nonlinear dynamically coupled models [e.g. Saha  
 126 et al. 2006]. The forecast skill of the correlation based models remains competitive with that of  
 127 comprehensive NWP models even on subseasonal time scales [Winkler et al. 2001; Newman et  
 128 al. 2003]. We provide further evidence below that (1) is a good enough approximation for the  
 129 evolution of monthly SST anomalies that  $\mathbf{L}$  provides useful information on both local and  
 130 remote SST feedbacks in the tropics.

131

132 We used the LIM formalism of Penland and Sardeshmukh [1995, hereafter PS95] to estimate  $\mathbf{L}$   
 133 from 3 observational and 76 coupled climate model simulation datasets of the 20<sup>th</sup> century. The  
 134 details of LIM may be found in PS95 and are not repeated here. Briefly,  $\mathbf{L}$  can be estimated  
 135 using the lag-covariance equation  $\mathbf{C}(\tau) = \exp(\mathbf{L}\tau) \mathbf{C}(0)$  satisfied by all dynamical systems of

136 the form (1) with  $\mathbf{F} = 0$ , where  $C_{ij}(\tau) = \langle x_i(t+\tau) x_j(t) \rangle$  are the elements of the lag covariance  
 137 matrix  $\mathbf{C}(\tau)$  at time lag  $\tau$ , by specifying  $\mathbf{C}(0)$  and  $\mathbf{C}(\tau_0)$  at some lag  $\tau_0$ . One can repeat this  
 138 exercise using other training lags  $\tau_0$ ; if the system is indeed of the form (1), then one should  
 139 obtain the same  $\mathbf{L}$ . This is the so-called "Tau test" of PS95 for the validity of linear  
 140 stochastically forced dynamics. Note that even though  $\mathbf{L}$  is estimated using covariances at  
 141 relatively short lags  $\tau_0$  (several months in our case) over which the changes of  $\mathbf{F}$  are presumed  
 142 to be negligible, this same  $\mathbf{L}$  can then be used to determine the system's response as  $\langle \mathbf{x} \rangle = -\mathbf{L}^{-1}\mathbf{F}$   
 143 to  $\mathbf{F}$  on long time scales.

144  
 145 Our use of LIM here is distinct from that in previous LIM studies [e.g., PS95; Penland and  
 146 Matrosova 1998; Winkler et al. 2001; Newman et al. 2003; Penland and Matrosova 2006,  
 147 Alexander et al. 2008, Newman et al. 2009], in which the emphasis was mainly on prediction and  
 148 predictability, and  $\mathbf{L}$  was estimated using observations projected onto a truncated EOF space.  
 149 Here, our emphasis is on intercomparing  $\mathbf{L}$  matrices estimated from observations and coupled  
 150 climate model simulations, and *in grid space*, to isolate inadequately modeled interactions  
 151 among specific geographical regions. Such a diagnosis is harder to interpret when performed in a  
 152 truncated EOF basis, mainly because the dominant EOFs of detrended tropical climate variations  
 153 are not geographically localized structures and account for different fractions of the SST  
 154 variance at different locations. Note that we retain *all* of the variance of the detrended area-  
 155 averaged monthly SST anomalies in each of our 8 localized regions. The SST anomalies in those  
 156 regions, obtained after removing the grand mean, mean annual cycle, and linear trend from the  
 157 100-yr monthly SST time series, define our 8-component state vector  $\mathbf{x}(t)$  in (1).

158

159 Despite the seemingly drastic approximations made in (1), estimates of  $\mathbf{L}$  from both the

160 observational and simulation SST datasets pass the "Tau test" remarkably well, as shown in Fig.

161 2. To generate the figure, we estimated  $\mathbf{L}$  from each dataset using training lags  $\tau_0$  ranging from

162 1 to at least 5 months. (As explained in PS95, a technical difficulty with LIM is that it fails to

163 estimate  $\mathbf{L}$ , *even if (1) is valid*, if  $\tau_0$  exceeds the half-period corresponding to the highest164 eigenfrequency of  $\mathbf{L}$ , i.e. beyond the Nyquist lag). The near-independence of  $\mathbf{L}$  on  $\tau_0$  may be165 gauged in Fig. 2 by the nearly constant magnitude of  $\mathbf{L}$  times a "representative" constant vector166  $\underline{\lambda}$  (whose 8 components are proportional to the SST standard deviations in the 8 regions) as  $\tau_0$ 167 is varied. The thick black and thin gray curves show the results for  $|\mathbf{L}\underline{\lambda}|$  obtained using the

168 observational and simulation datasets, respectively. It is reassuring that both sets of curves are

169 approximately flat, especially for  $\tau_0$  between 1 and 5 months, attesting to the validity of (1).

170 However, the model curves are vertically offset with respect to not only the observational but

171 also other model curves, and also generally terminate at different values of  $\tau_0$ . These results

172 suggest that the SST feedbacks are indeed effectively linear in both the observations and the

173 models, but the simulated  $\mathbf{L}$  matrices differ substantially from the observational matrices and

174 also from one another. We explore these errors and differences in greater detail below.

175

176 **3. Observed and simulated feedback matrices**177 Equation (1) may be cast in a standardized form by normalizing each component of  $\mathbf{x}$  by its178 standard deviation. The  $\mathbf{L}$  matrix then transforms into  $\hat{\mathbf{L}} = \mathbf{s}\mathbf{L}\mathbf{s}^{-1}$ , where  $\mathbf{s}$  is a diagonal matrix179 of the reciprocals of the SST standard deviations. Note that each element  $\hat{L}_{ij}$  of  $\hat{\mathbf{L}}$  has units of

180 inverse time (month<sup>-1</sup> in our case), and thus identifies a characteristic time scale for the influence  
 181 of an SST anomaly in region  $j$  on the anomaly in region  $i$ .

182

183 Figure 3 provides a detailed intercomparison of the observed and simulated  $\hat{\mathbf{L}}$  matrices. At each  
 184  $(i,j)$  location on the plot, the gray horizontal line segments show estimates of  $\hat{L}_{ij}$  from the 76  
 185 individual model simulations. The mean value and range of the corresponding 3 observational  
 186  $\hat{L}_{ij}$  estimates are indicated by the position and width of the red rectangle below the horizontal  
 187 axis. The multi-model ensemble mean of  $\hat{L}_{ij}$  is also shown below the horizontal axis as a filled  
 188 blue circle, together with two different measures of simulated uncertainty: the multi-model  
 189 ensemble spread of  $\hat{L}_{ij}$  ( $\pm \sigma_{\text{ALL}}$ ; outer blue bars), and the average of the “internal” ensemble  
 190 spread obtained for specific models with at least 3 ensemble members<sup>1</sup> ( $\pm \sigma_{\text{INT}}$ ; shorter inner  
 191 blue bars). In essence,  $\sigma_{\text{INT}}$  is a measure of the consistency of  $\hat{L}_{ij}$  estimated using different  
 192 simulations of the same model. The fact that  $\sigma_{\text{INT}}$  is generally much smaller than  $\sigma_{\text{ALL}}$  in Fig. 3  
 193 suggests that most of the multi-model spread of the  $\hat{L}_{ij}$  estimates arises from actual model  
 194 differences, rather than sampling error.

195

196 Figure 3 shows that to a first approximation, monthly SST anomalies throughout the tropics are  
 197 strongly damped by local interactions within the air-sea column, as indicated by the  
 198 predominantly negative values of the diagonal elements  $\hat{L}_{ii}$  of  $\hat{\mathbf{L}}$  in both observations and

---

<sup>1</sup> In clustering the coupled models, different versions of a model (including different resolution versions) from the same modeling group were treated separately. We determined a total of 14 such distinct model clusters. They are indicated by the right-handed brackets at the far right edge of the plot.

199 models. (Note that the scale for the diagonal elements in the figure is twice that for the off-  
 200 diagonal elements). This local damping time scale is relatively short ( $\sim 4$  months) in the Indian  
 201 and Western Pacific (Regions 1-3), somewhat longer ( $\sim 6$  months) in the Atlantic (Regions 7-8),  
 202 and relatively long (6 to 9 months) in the eastern Pacific (Regions 4-6) basins. It is longest in the  
 203 Cold Tongue "ENSO" region of the eastern equatorial Pacific (Region 5). The multi-model  
 204 ensemble mean values of  $\hat{L}_{ii}$  are generally in reasonable agreement with the observed values,  
 205 although there is considerable inter-model spread that is largest (relative to the ensemble-mean  
 206 value) in the ENSO Region 5. The positive bias of the models'  $\hat{L}_{55}$  with respect to the observed  
 207 (indicative of weaker than observed local damping) is also relatively the largest. A similar weak  
 208 local damping bias was implicated by Sun et al. (2006) in the excessive coldness of the long-  
 209 term mean SSTs in this region in a smaller group of coupled model simulations. Apparently the  
 210 spuriously weak damping of SSTs in the ENSO region remains a prevalent problem.

211  
 212 Given the importance of ENSO, the remote influence on the ENSO region from other regions  
 213 ( $\hat{L}_{5j}$ ), as well as the influence of the ENSO region on the other regions ( $\hat{L}_{is}$ ) are of particular  
 214 interest. These interactions are highlighted by the green and yellow colored 5th row and 5th  
 215 column, respectively, of  $\hat{\mathbf{L}}$  in Fig. 3. Significant model misrepresentations of the remote impacts  
 216 on the ENSO region ( $\hat{L}_{5j}$ ) are evident, consistent with the suggestion from previous studies that  
 217 simulation errors outside the Pacific basin also contribute substantially to errors in ENSO  
 218 simulations [e.g. Guilyardi et al. 2009]. For instance, the damping impact of Indian Ocean SSTs  
 219 on ENSO suggested in many studies [e.g. Annamalai et al. 2005; Kug and Kang 2006; Kug et al.  
 220 2006; Dommenges et al. 2006; Yeh et al. 2007] is clear in both our observational and model

221 based  $\hat{L}_{5j}$  estimates; however, the exact locations of the influential regions are different.  
 222 Whereas the models are in unanimous agreement that the damping influence is exerted from the  
 223 entire Indian Ocean basin, the observations are equally unanimous in suggesting that it is exerted  
 224 only from the eastern half of the basin. Indeed, the observations suggest a *positive* feedback on  
 225 ENSO by SSTs in the western Indian Ocean ( $\hat{L}_{51}\hat{L}_{15} > 0$ ), in sharp contrast to the negative  
 226 feedback in the models. The models also misrepresent the influence of the Atlantic SSTs on the  
 227 ENSO region. The observations suggest a very weak influence, whereas the models suggest a  
 228 substantial influence, but with little inter-model agreement even with regard to the sign of the  
 229 North Atlantic influence ( $\hat{L}_{57}$ ). And finally, Figure 3 provides evidence that the influence of the  
 230 northern off-equatorial SSTs on the equatorial SSTs in Region 5 ( $\hat{L}_{54}$ ) is systematically too  
 231 strong in the models compared to observations.

232

233 Several aspects of the impact of SSTs in the ENSO region on other regions ( $\hat{L}_{i5}$ ) are also not  
 234 well captured by the coupled models. For instance, the impacts on the eastern Indian ( $\hat{L}_{25}$ ) and  
 235 southern tropical Atlantic oceans ( $\hat{L}_{85}$ ) are clearly outside the range of the observational  
 236 estimates. Also, there is strong inter-model disagreement concerning even the sign of the impact  
 237 on the Warm Pool SSTs ( $\hat{L}_{25}$ ,  $\hat{L}_{35}$ ). With regard to the impact on SSTs in the regions to the  
 238 immediate north and south of the ENSO region, the models suggest a large positive impact on  
 239 both regions ( $\hat{L}_{45} > 0$  and  $\hat{L}_{65} > 0$ ), whereas the observations suggest a large impact only on the  
 240 southern region ( $\hat{L}_{65} > 0$ ).

241

242 Besides interactions with the ENSO region, Fig. 3 suggests significant model misrepresentations  
243 of the Indian ocean influences on the southern Atlantic basin ( $\hat{L}_{81}$  and  $\hat{L}_{82}$ ); the western Pacific  
244 influences on the Eastern Indian ( $\hat{L}_{23}$ ), northeastern Pacific ( $\hat{L}_{43}$ ), southeastern Pacific ( $\hat{L}_{63}$ ) and  
245 southern Atlantic ( $\hat{L}_{83}$ ) basins; the northeastern Pacific influence on the western Pacific ( $\hat{L}_{34}$ )  
246 basin; and the northern Atlantic influence on the western Indian ( $\hat{L}_{17}$ ) and northeastern and  
247 southeastern Pacific ( $\hat{L}_{47}$  and  $\hat{L}_{67}$ ) basins. In many instances these influences are inconsistent  
248 even with regard to sign among the models.

249

#### 250 **4. Summary and discussion**

251 In this study we investigated the interactions among 8 broadly defined regions of coherent  
252 tropical SST variability in the Pacific, Indian, and Atlantic Ocean basins using 3 observational  
253 and 76 climate model simulation datasets of the 20<sup>th</sup> century. The 8-dimensional SST feedback  
254 matrix was estimated separately using each dataset by constructing a Linear Inverse Model based  
255 on the lag-covariance statistics of the 100-yr monthly SST time series. In general, we found the  
256 local feedbacks on SST in our 8 selected regions to be reasonably consistent among the  
257 observations and the coupled models, although relatively less so in the eastern equatorial ENSO  
258 region (Region 5). It was in the representation of the *remote* feedbacks that we found the models  
259 differing most from the observations, and also from one another. In particular, we found the  
260 influence of the eastern Pacific ENSO region on other regions, and of the other regions on the  
261 ENSO region, to vary considerably from model to model. We also found the representation of  
262 remote interactions with the Indo-Pacific Warm Pool region to be highly variable.

263

264 Figure 3 provides a comprehensive summary of the results from our local and remote feedback  
265 analysis. It depicts the realism or otherwise of coupled model representations of all possible  
266 interactions among our 8 selected regions of dominant tropical SST variability. Although our  
267 emphasis was on highlighting those interactions that are represented particularly poorly in the  
268 models, the dominant impression from the figure is that of large inter-model inconsistencies in  
269 the remote feedbacks even in instances when the multi-model ensemble-mean feedback is in  
270 reasonable agreement with the observations.

271

272 Given such model errors and inconsistencies in the feedback operator  $\mathbf{L}$ , relying on any one  
273 particular climate model to generate realistic responses  $\langle \mathbf{x} \rangle = -\mathbf{L}^{-1}\mathbf{F}$  to external radiative forcing  
274 is clearly unjustified. Focusing on the multi-model ensemble mean response  $\overline{\langle \mathbf{x} \rangle} = -\overline{\mathbf{L}}^{-1}\mathbf{F}$  is the  
275 usual suggested solution to this problem. However, we have provided evidence that even the  
276 multi-model mean operator  $\overline{\mathbf{L}}$  differs from the observed operator in several key respects. The  
277 conclusion seems inescapable that at the very least, some important elements of  $\overline{\mathbf{L}}$  highlighted in  
278 this paper should agree better with observations to increase our confidence in the ability of even  
279 a multi-model ensemble to generate reliable responses to external forcing. Reduction of  
280 interaction errors that are systematic across all the models in Fig. 3 would appear to be an  
281 obvious first step. The fact that such interactions, especially among basins separated by  
282 continental land masses, generally occur on time scales of at most a few months suggests that  
283 they occur primarily through the atmosphere and not through the oceans, which should help in  
284 error diagnosis and reduction.

285

286 We end by pointing to an encouraging aspect of isolating model errors at the level of the  
287 feedback operator  $\mathbf{L}$ , as done here, as opposed to merely documenting long-term simulation  
288 errors to demonstrate the existence of model errors. This is that the model errors in  $\mathbf{L}$  should be  
289 manifested in errors of tropical SST forecasts made using the models at forecast ranges of as  
290 short as one month, given the validity of (1) even at this short range as demonstrated in Fig. 2.  
291 This suggests that an extensive model improvement program involving even very large numbers  
292 of short ( $\sim 1$  month) experimental model integrations to diagnose and reduce the short-range SST  
293 forecast errors and, concurrently, errors in  $\mathbf{L}$ , might prove fruitful.

294

295 **Acknowledgments.** This work was supported by a grant from NOAA's Climate Variability  
296 and Predictability (CVP) Program.

297

297 **References**

- 298 Alexander, M. A., I. Blade, M. Newman, J. R. Lanzante, N.-C. Lau, and J. D. Scott (2002), The  
 299 atmospheric bridge: The influence of ENSO teleconnections on air-sea Interaction over  
 300 the global oceans, *J. Climate*, *15*, 2205-2231.  
 301
- 302 Alexander, M. A., L. Matrosova, C. Penland, J. D. Scott, and P. Chang (2008), Forecasting  
 303 pacific SSTs: Linear Inverse Model predictions of the PDO, *J. Climate*, *21*, 385-402.  
 304
- 305 Annamalai, H., S. P. Xie, J. P. McCreary, and R. Murtugudde (2005), Impact of Indian Ocean  
 306 sea surface temperature on developing El Niño, *J. Climate*, *18*, 302-319.  
 307
- 308 Barsugli J. J., and D. S. Battisti (1998), The basic effects of atmosphere–ocean thermal coupling  
 309 on midlatitude variability, *J. Atmos. Sci.*, *55*, 477–493.  
 310
- 311 Barsugli. J. J., and P. D. Sardeshmukh (2002), Global atmospheric sensitivity to tropical SST  
 312 anomalies throughout the Indo-Pacific Basin, *J. Climate*, *15*, 3427-3442.  
 313
- 314 Barsugli J. J., S.-I. Shin, and P. D. Sardeshmukh (2006), Sensitivity of global warming to the  
 315 pattern of tropical ocean warming, *Clim. Dyn.*, *27*, 483-492.  
 316
- 317 Cash, B. A., E. K. Schneider, and L. Bengtsson (2005), Origin of regional climate differences:  
 318 role of boundary conditions and model formulation in two GCMs, *Clim. Dyn.*, *25*, 709-  
 319 723.  
 320
- 321 Dommenget, D., V. Semenov, and M. Latif (2006), Impacts of the tropical Indian and Atlantic  
 322 Oceans on ENSO, *Geophys. Res. Lett.*, *33*, L11701, doi:10.1029/2006GL025871.  
 323
- 324 Enfield, D. B., and D. A. Mayer (1997), Tropical Atlantic sea surface temperature variability and  
 325 its relation to El Niño-Southern Oscillation, *J. Geophys. Res.*, *102*, 929– 946.  
 326
- 327 Frankignoul, C. (1985), Sea surface temperature anomalies, planetary waves, and air-sea  
 328 feedback in the middle latitudes, *Rev. Geophys.*, *23*, 357–390.  
 329
- 330 Giannini, A., R. Saravanan, and P. Chang (2004), The preconditioning role of Tropical Atlantic  
 331 variability in the development of the ENSO teleconnection: Implications for the  
 332 prediction of Nordeste rainfall. *Clim. Dyn.*, *22*, 839-855.  
 333
- 334 Guilyardi, E., and Coauthors (2009), Understanding El Niño in ocean-atmosphere general  
 335 circulation models: Progress and challenges, *Bull. Amer. Meteor. Soc.*, *90*, 325-340.  
 336
- 337 Hasselmann, K. (1976), Stochastic climate models. Part I. Theory, *Tellus*, *28*, 473–484.  
 338
- 339 IPCC (2007), Climate Change 2007: The Physical Science Basis. Contribution of Working  
 340 Group I to the Fourth Assessment Report of the Intergovernmental Panel on Climate  
 341 Change [Solomon, S., D. Qin, M. Manning, Z. Chen, M. Marquis, K. B. Averyt, M.

- 342 Tignor, and H. L. Miller (eds.)], Cambridge University Press, Cambridge, United  
343 Kingdom and New York, pp. 996.  
344
- 345 Kaplan, A., M. Cane, Y. Kushnir, A. Clement, M. Blumenthal, and B. Rajagopalan (1998),  
346 Analyses of global sea surface temperature 1856-1991, *J. Geophys. Res.*, *103*, 18567-  
347 18589.  
348
- 349 Klein, S. A., Soden, B. J., and N.-C. Lau (1999), Remote sea surface temperature variations  
350 during ENSO: Evidence for a tropical atmospheric bridge, *J. Climate*, *12*, 917-932.  
351
- 352 Knutson, T. R., and Coauthors (2006), Assessment of Twentieth-Century regional surface  
353 temperature trends using the GFDL CM2 coupled models, *J. Climate*, *19*, 1624-1651.  
354
- 355 Kug, J. S., and I. S. Kang (2006), Interactive Feedback between ENSO and the Indian Ocean. *J.*  
356 *Climate*, *19*, 1784-1801.  
357
- 358 Kug, J. S., Kirtman, B. P., and I. S. Kang (2006), Interactive Feedback between ENSO and the  
359 Indian Ocean in an Interactive Ensemble Coupled Model. *J. Climate*, *19*, 6371-6381.  
360
- 361 Lin, J. L. (2007), The double-ITCZ problem in IPCC AR4 coupled GCMs: Ocean-atmosphere  
362 feedback analysis, *J. Climate*, *20*, 4497-4525.  
363
- 364 Meehl, G. A., W. M. Washington, J. M. Arblaster, and A. Hu (2004), Factors affecting climate  
365 sensitivity in coupled models, *J. Climate*, *17*, 1584-1596.  
366
- 367 Newman, M., P. D. Sardeshmukh, C. R. Winkler, and J. S. Whitaker (2003), A study of  
368 subseasonal predictability, *Mon. Wea. Rev.*, *131*, 1715-1732.  
369
- 370 Newman, M., P. D. Sardeshmukh, and C. Penland (2009), How important is air-sea coupling in  
371 ENSO and MJO evolution? *J. Climate*, *22*, 2958-2977.  
372
- 373 Penland, C., and P. D. Sardeshmukh (1995), The optimal growth of tropical sea surface  
374 temperature anomalies, *J. Climate*, *8*, 1999-2024.  
375
- 376 Penland, C., and L. Matrosova (1998), Prediction of tropical Atlantic sea surface temperatures  
377 using Linear Inverse Modeling, *J. Climate*, *11*, 483-496.  
378
- 379 Penland, C., and L. Matrosova (2006), Studies of El Nino and interdecadal variability in tropical  
380 sea surface temperatures using a nonnormal filter, *J. Climate*, *19*, 5796-5815.  
381
- 382 Rayner, N. A., and Coauthors (2003), Global analyses of sea surface temperature, sea ice, and  
383 night marine air temperature since the late nineteenth century, *J. Geophys. Res.*, *108*,  
384 4407, doi:10.1029/2002JD002670.  
385
- 386 Saha, S., and Coauthors (2006), The NCEP Climate Forecast System, *J. Climate*, *19*, 3483-3517.  
387

- 388 Schneider, E. K., L. Bengtsson, and Z.-Z. Hu (2003), Forcing of Northern Hemisphere climate  
389 trends, *J. Atmos. Sci.*, *60*, 1504-1521.  
390
- 391 Smith T. M. and R. W. Reynolds (2005), A global merged land-air-sea surface temperature  
392 reconstruction based on historical observations (1880-1997), *J. Climate*, *18*, 2021-2036.  
393
- 394 Sun, D.-Z., T. Zhang, C. Covey, S. Klein, W. D. Collins, J. J. Hack, J. T. Kiehl, G. A. Meehl, I.  
395 M. Held, and M. Suarez (2006), Radiative and dynamical feedbacks over the equatorial  
396 cold-tongue: Results from nine atmospheric GCMs, *J. Climate* , *19*, 4059-4074.  
397
- 398 Winkler, C. R., Newman, M., and P. D. Sardeshmukh (2001), A linear model of wintertime low-  
399 frequency variability. Part I: Formulation and forecast skill, *J. Climate*, *14*, 4474-4494.  
400
- 401 Yeh, S.-W., R. Wu, and B. P. Kirtman (2007), Impact of the Indian Ocean on ENSO variability  
402 in a hybrid coupled model, *Q. J. R. Meteorol. Soc.*, *133*, 445-457.  
403
- 404 Yu, J.-Y., C. R. Mechoso, J. C. McWilliams, and A. Arakawa (2002), Impacts of the Indian  
405 Ocean on the ENSO cycle, *Geophys. Res. Lett.*, *29*, 1204, doi:10.1029/2001GL014098.  
406

406 **Figure Legends**

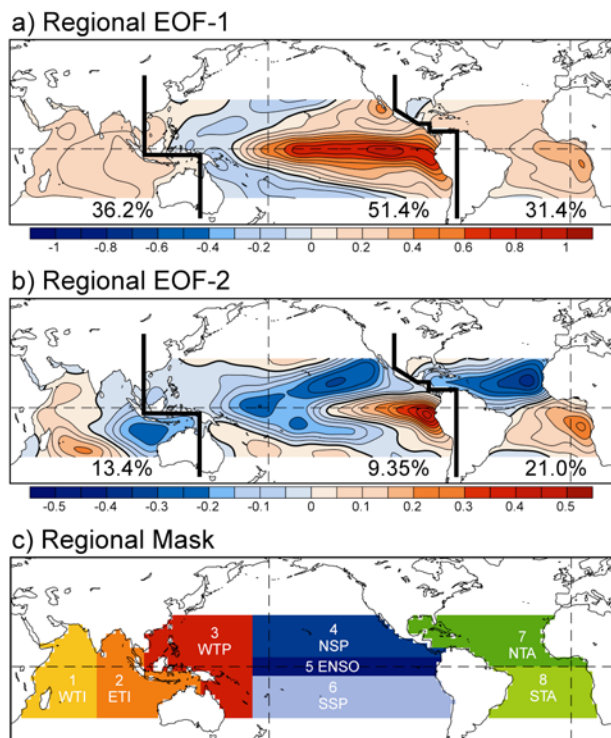
407 **Fig. 1** (a) The dominant regional EOFs of monthly SST anomalies in the tropical Indian, Pacific,  
 408 and Atlantic Oceans obtained from separate EOF analyses and shown in the same map for ease  
 409 of presentation. The regional boundaries of the EOF analyses are indicated by thick black lines.  
 410 The numbers along the bottom indicate the fractions of SST variance explained by the EOFs. (b)  
 411 As in (a) but for the second most dominant EOFs. The SST data are from the 20<sup>th</sup> century (1900-  
 412 1999) HadISST data set [Rayner et al. 2003]. The data were interpolated to a T42 Gaussian grid  
 413 before performing the EOF analyses. The raw EOF patterns obtained were then spatially  
 414 smoothed using a T21 spectral filter to emphasize the larger scale features. (c) Our 8 selected  
 415 tropical regions of geographically coherent SST variability based upon the EOF analyses. Region  
 416 1: WTI (Western Tropical Indian), Region 2: ETI (Eastern Tropical Indian), Region 3: WTP  
 417 (Western Tropical Pacific), Region 4: NSP (North Subtropical Pacific), Region 5: ENSO, Region  
 418 6: SSP (South Subtropical Pacific), Region 7: NTA (North Tropical Atlantic), and Region 8:  
 419 STA (South Tropical Atlantic).

420

421 **Fig. 2** The dependence of the magnitude  $|\mathbf{L}\underline{\lambda}|$  of the effective SST feedback matrix  $\mathbf{L}$  times a  
 422 “representative” constant vector  $\underline{\lambda}$ , on the training lag  $\tau_0$  used for estimating  $\mathbf{L}$ . Results are  
 423 shown for  $\mathbf{L}$  estimated using 3 observational (thick black curves) and 76-coupled simulation  
 424 (thin gray curves) datasets. Note that although the model results differ substantially from the  
 425 tightly clustered observational results, the curves for both observations and models are  
 426 approximately flat for  $\tau_0$  between 1 and 5 months (demarcated by light gray shading).

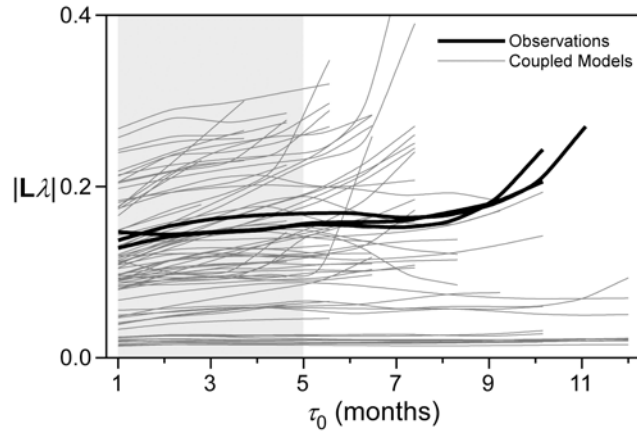
427

428 **Fig. 3** Intercomparisons of the elements of the standardized 8 x 8 effective linear dynamical  
429 feedback matrix  $\hat{\mathbf{L}}$  (units: month<sup>-1</sup>) estimated using 3 observational and 76 climate model  
430 simulation datasets. For each matrix element  $(i,j)$ , the gray bars show  $\hat{L}_{ij}$  estimated using the 76  
431 individual simulations. The multi-model ensemble mean  $\hat{L}_{ij}$  is indicated by the blue dot below  
432 the horizontal axis, along with the multi-model ensemble spread of  $\hat{L}_{ij}$  among all 76 simulations  
433 ( $\pm\sigma_{\text{ALL}}$ ; large outer blue bars), and the average of the internal ensemble spread of  $\hat{L}_{ij}$  obtained  
434 in 14 subsets of the ensemble simulations, each containing least 3 ensemble members, generated  
435 using distinct models ( $\pm\sigma_{\text{INT}}$ ; smaller inner blue bars). The mean value and range of  $\hat{L}_{ij}$   
436 estimated using the 3 observational datasets are indicated by the position and width of the red  
437 rectangles below the horizontal axis.  $\hat{L}_{ij}$  is a measure of the direct influence of the standardized  
438 SST anomalies in region  $j$  on the standardized SST anomalies in region  $i$  (see Fig. 1 for  
439 locations). The influences on the equatorial eastern Pacific “ENSO” Region 5 from the other  
440 regions ( $\hat{L}_{5j}$ ), and the influences of the ENSO region on the other regions ( $\hat{L}_{i5}$ ), are highlighted  
441 by the green colored 5<sup>th</sup> row and yellow colored 5<sup>th</sup> column, respectively, of  $\hat{\mathbf{L}}$ . See text for  
442 further details.  
443



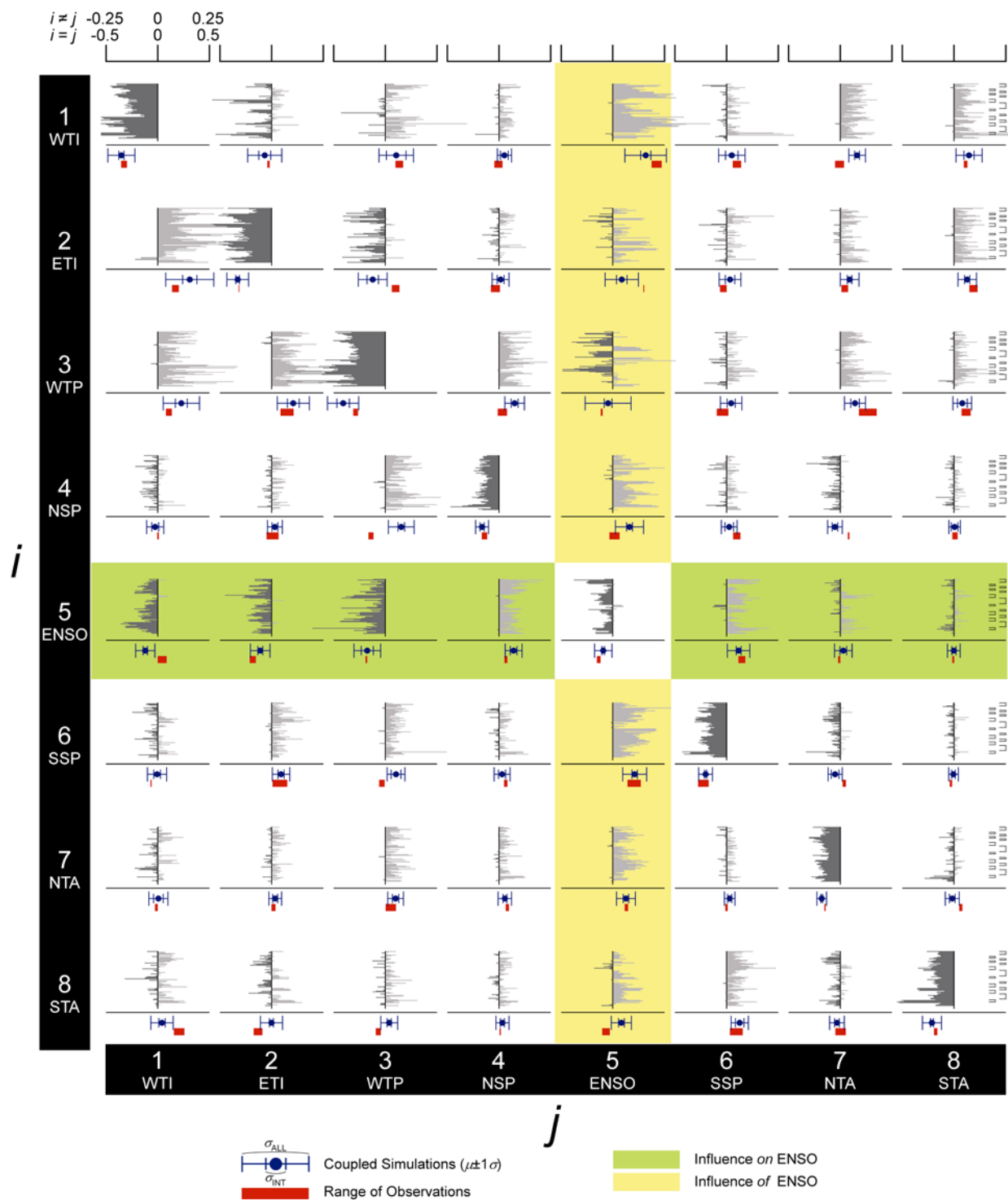
443

444 **Fig. 1** (a) The dominant regional EOFs of monthly SST anomalies in the tropical Indian, Pacific, and  
 445 Atlantic Oceans obtained from separate EOF analyses and shown in the same map for ease of  
 446 presentation. The regional boundaries of the EOF analyses are indicated by thick black lines. The  
 447 numbers along the bottom indicate the fractions of SST variance explained by the EOFs. (b) As in (a) but  
 448 for the second most dominant EOFs. The SST data are from the 20<sup>th</sup> century (1900-1999) HadISST data  
 449 set [Rayner et al. 2003]. The data were interpolated to a T42 Gaussian grid before performing the EOF  
 450 analyses. The raw EOF patterns obtained were then spatially smoothed using a T21 spectral filter to  
 451 emphasize the larger scale features. (c) Our 8 selected tropical regions of geographically coherent SST  
 452 variability based upon the EOF analyses. Region 1: WTI (Western Tropical Indian), Region 2: ETI  
 453 (Eastern Tropical Indian), Region 3: WTP (Western Tropical Pacific), Region 4: NSP (North Subtropical  
 454 Pacific), Region 5: ENSO, Region 6: SSP (South Subtropical Pacific), Region 7: NTA (North Tropical  
 455 Atlantic), and Region 8: STA (South Tropical Atlantic).  
 456



456

457 **Fig. 2** The dependence of the magnitude  $|\mathbf{L}\underline{\lambda}|$  of the effective SST feedback matrix  $\mathbf{L}$  times a  
 458 “representative” constant vector  $\underline{\lambda}$ , on the training lag  $\tau_0$  used for estimating  $\mathbf{L}$ . Results are shown for  
 459  $\mathbf{L}$  estimated using 3 observational (thick black curves) and 76-coupled simulation (thin gray curves)  
 460 datasets. Note that although the model results differ substantially from the tightly clustered observational  
 461 results, the curves for both observations and models are approximately flat for  $\tau_0$  between 1 and 5  
 462 months (demarcated by light gray shading).  
 463



463

464 **Fig. 3** Intercomparisons of the elements of the standardized 8 x 8 effective linear dynamical feedback  
 465 matrix  $\hat{\mathbf{L}}$  (units: month<sup>-1</sup>) estimated using 3 observational and 76 climate model simulation datasets. For  
 466 each matrix element  $(i,j)$ , the gray bars show  $\hat{L}_{ij}$  estimated using the 76 individual simulations. The  
 467 multi-model ensemble mean  $\hat{L}_{ij}$  is indicated by the blue dot below the horizontal axis, along with the

468 multi-model ensemble spread of  $\hat{L}_{ij}$  among all 76 simulations ( $\pm\sigma_{\text{ALL}}$ ; large outer blue bars), and the  
 469 average of the internal ensemble spread of  $\hat{L}_{ij}$  obtained in 14 subsets of the ensemble simulations, each  
 470 containing least 3 ensemble members, generated using distinct models ( $\pm\sigma_{\text{INT}}$ ; smaller inner blue bars).  
 471 The mean value and range of  $\hat{L}_{ij}$  estimated using the 3 observational datasets are indicated by the  
 472 position and width of the red rectangles below the horizontal axis.  $\hat{L}_{ij}$  is a measure of the direct influence  
 473 of the standardized SST anomalies in region  $j$  on the standardized SST anomalies in region  $i$  (see Fig. 1  
 474 for locations). The influences on the equatorial eastern Pacific “ENSO” Region 5 from the other regions  
 475 ( $\hat{L}_{5j}$ ), and the influences of the ENSO region on the other regions ( $\hat{L}_{i5}$ ), are highlighted by the green  
 476 colored 5<sup>th</sup> row and yellow colored 5<sup>th</sup> column, respectively, of  $\hat{\mathbf{L}}$ . See text for further details.